Environmental Earth Sciences (2023) 82:82
https://doi.org/10.1007/s12665-023-10779-5

ORIGINAL ARTICLE

Numerical investigation of processes, features, and control of land subsidence caused by groundwater extraction and coal mining: a case study from eastern China

Zhiqiang Li[1,2,4] · Qiqi Chen[2,5] · Yiguo Xue[2,3] · Daohong Qiu[2] · Hong Chen[2] · Fanmeng Kong[2,3] · Qiushi Liu[2]

Received: 19 July 2022 / Accepted: 16 January 2023 / Published online: 28 January 2023

Abstract

Land subsidence is a typical geological disaster that will produce many secondary disasters and negatively impact human production and life. Human engineering activities (underground mining and coal mining) are the leading causes of land subsidence. This study takes Jining, a typical land subsidence city in eastern China, as a case study to investigate the features and control of land subsidence under the combined action of groundwater extraction and coal mining. A three-dimensional numerical model of land subsidence considering groundwater extraction and coal mining is established. The evolution process of land subsidence in the study area from 2000 to 2020 under the action of groundwater extraction and coal mining was obtained through numerical simulation. Results showed that coal mining was the main cause of land subsidence compared to groundwater extraction in the study area. Different groundwater extraction schemes were proposed to try to control the land subsidence, and the land subsidence features of different schemes from 2021 to 2030 were also investigated. Results showed that the ground rebound phenomenon occurred during the first few years, and the rate and amount of ground rebound decreased over time. After that, land subsidence continued, and its rate gradually slowed. The more mining wells are shut down, the smaller the final cumulative land subsidence will be. According to the comparison of these schemes, the land subsidence is basically stable when the amount of groundwater exploitation wells is closed by 50%, which is a more reasonable and practical exploitation scheme.

Keywords Land subsidence · Groundwater extraction · Coal mining · Subsidence control · Numerical simulation

Introduction

Land subsidence is the phenomenon that the ground elevation in a specific area gradually decreases due to the consolidation and compression of the loose layers under the action of natural factors or human activities(Holzer and Galloway 2005; Peng et al. 2016). The earliest record of land subsidence in the world was in Mexico in 1891(Mehdi et al. 2021), and the earliest history of land subsidence in China was in Shanghai in 1921(Xue et al. 2005). With the advancement of urbanization and the increase in population, human demand for natural resources continues to expand, which makes land subsidence continue to increase(Gerardo et al. 2021). There are serious land subsidence problems in many cities and regions worldwide, such as Beijing, Shanghai, Shandong, California, Mexico City, Tokyo, Osaka, Venice, Bangkok, etc. Land subsidence has become a global problem(Chen et al. 2017; Gerardo et al. 2021; Phien-wej et al. 2006; Shen and Xu 2011).

✉ Zhiqiang Li
zhiqiangli@sdu.edu.cn

1 Shandong Provincial Lunan Geology and Exploration Institute (Shandong Provincial Bureau of Geology and Mineral Resources No.2 Geological Brigade), Jining 272000, Shandong, China

2 Geotechnical and Structural Engineering Research Center, Shandong University, Jinan 250061, Shandong, China

3 School of Engineering and Technology, China University of Geosciences (Beijing), Beijing 100083, China

4 Technology Innovation Center of Restoration and Reclamation in Mining Induced Subsidence Land, Ministry of Natural Resources, Jining 272000, Shandong, China

5 China Construction Eighth Bureau, Zhejiang Construction Co., Ltd., Hangzhou 310000, Zhejiang, China

The natural factors caused land subsidence include tectonic movement, compaction, and consolidation of the soil layer due to its weight. The human factors caused land subsidence include over-exploitation of groundwater, over-exploitation of underground hot springs, over-exploitation of oil and natural gas resources, and underground engineering construction, etc. (Dehghani et al. 2008; Ebrahimy et al. 2020; Zhang et al. 2019). Different regions and cities have different causes of land subsidence, so they have different distribution characteristics and evolution laws of land subsidence (Edalat et al. 2020; Hu et al. 2004; Mehdi et al. 2021)。

The North China Plain is one of China's three major land subsidence areas(Xue et al. 2005). Large-scale land subsidence has continued to occur since the 1950s. The impact of tectonic activities on land subsidence is limited. Human factors, especially deep groundwater extraction and coal mining, are the main reasons for land subsidence in the North China Plain (Chen et al. 2019; Di et al. 2020; Hu et al. 2004). The over-exploitation of groundwater has deteriorated the hydrogeological conditions of the North China Plain, and the high-intensity exploitation of groundwater has caused the groundwater level to drop. Many adverse environmental and geological problems have been derived. Among them, land subsidence is the most prominent threat. Its damage involves a wide range, takes a long time, and is even irreversible. It threatens human production and life and affects social and economic development(Chen et al. 2017, 2019; Guzy and Witkowski 2021; Shen and Xu 2011).

Currently, theoretical analysis and numerical simulation have been carried out on land subsidence induced by single factors such as groundwater extraction and coal mining(Edalat et al. 2020; Guzy and Malinowska 2020a, b; Guzy and Witkowski 2021; Shen and Xu 2011; Yang et al. 2015). However, the land subsidence caused by the joint/coupling action of two or more factors is still in its infancy(Ding et al. 2020; Jia et al. 2021). Based on the random medium theory and superposition principle, (Liu et al. 1999) deduced the calculation formula of land subsidence for open-air excavation and hydrophobicity of rock and soil. (Jia et al. 2021)analyzed the land subsidence caused by coal mining and groundwater extraction based on the Biot's consolidation theory and numerical model and analyzed its impact on high-speed rail. (Guzy and Witkowski 2021) explored the land subsidence caused by groundwater withdrawal induced by mining through numerical simulation. At present, the research on land subsidence under the action of multi-field coupling has gradually become an important research direction, and there are few studies on land subsidence caused by two or more factors.

Taking the land subsidence area in Jining City, China, as a case study, this research employed numerical simulation and field monitoring to study the characteristics of land subsidence under the combined action of groundwater and coal mining and explored effective methods for controlling land subsidence. Based on the study area's hydrogeological and engineering geological data and Biot's consolidation theory, a fluid–solid coupling numerical model of land subsidence in the study area was established to restore the evolution processes and features of land subsidence caused by groundwater extraction and coal mining. The trend of land subsidence under different schemes was predicted by designing various groundwater extraction schemes. The research results can not only provide a theoretical basis and data support for the prevention and control of land subsidence in this area, but also propose effective prevention and control measures in a targeted manner.

Study background

Study area

Jining City locates at the southernmost end of the North China Plain and is rich in groundwater resources and coal reserves. Groundwater extraction and coal mining are the main reasons for its land subsidence. The initial stage of land subsidence is mainly caused by high-intensity groundwater extraction and the center of the subsidence trough shifts with the distribution of mining wells. With the rapid growth of coal production after the 1990s, the problem of land subsidence caused by coal mining continues to intensify. Land subsidence results in damage to farmland, seepage of groundwater, and the formation of large-scale subsidence and stagnant water, thus posing a threat to people's life, property safety, and social and economic development.

The study area is located in the middle of Jining City, Shandong Province, China, with an area of about 207 km^2 (blue area in Fig. 1). The terrain of the study area is flat and

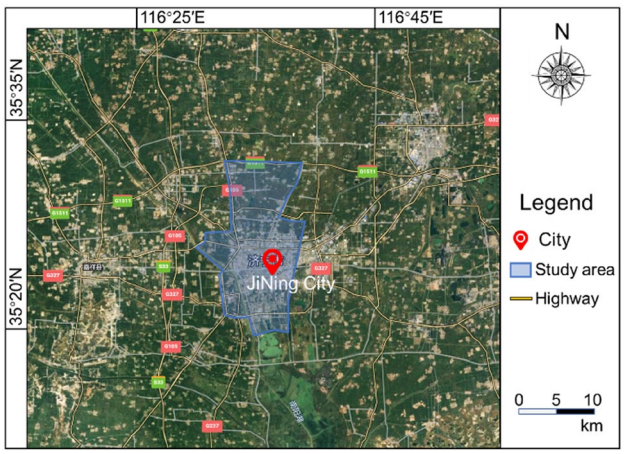

Fig.1 Position of the study area

open. Various landforms include low mountains and hills, plain depressions, and lakeside depressions. As a typical land subsidence area, groundwater extraction and coal mining are the leading causes of land subsidence, especially the overlapping area of groundwater extraction and coal mining.

Stratigraphic lithology

The stratum in the study area develops from old to new: Paleozoic Ordovician, Carboniferous-Permian, Mesozoic Jurassic, and Cenozoic Quaternary. The Ordovician is mainly the Majiagou Group, with a thickness of about 500–742 m. And the lithology is primarily limestone, dolomitic limestone, and marl. The Carboniferous-Permian is mainly the Yuemengou Group, with a thickness of 43.00–70.50 m and an average thickness of 60.30 m. The lithology comprises variegated, aluminous mudstone, grey-green claystone, and limestone. The Jurassic is mainly the Sandai Formation of the Zibo Group, with a thickness of 240.20–641.20 m. The lithology is primarily sandstone, siltstone interbedded with conglomerate and coal rock, where artificial mining activities are frequent.

The uppermost Cenozoic Quaternary loose layer has a thickness of 220–300 m, and the lithology is formed by the alternating accumulation of cohesive soil and sandy soil. The topsoil layer is the Quaternary Holocene loose cohesive soil layer with a thickness of 2–10 m. Down to 60–120 m, the Quaternary Pleistocene clay soil and sand-gravel layers alternately accumulated, during which 4–7 water-bearing sand layers developed. Vertically, the water-bearing sand layers mainly concentrate on two relatively enriched sand layers with a buried depth of 10–40 m and below 60 m.

The stratum can be divided into seven engineering geological layers according to the sedimentary sequence, water-rich and water-conducting properties, namely, the topsoil layer, the first compression layer, the first water-bearing sand layer group, the second compression layer, and the second water-bearing sand layer Formation, semi-cemented layer, bedrock. The topsoil layer is the Quaternary Holocene alluvial and lacustrine facies sediments, with a thickness of 2–10 m. The first compression layer comprises Pleistocene alluvial-pluvial layers with a thickness of 10–25 m. The I water-bearing sand layer group is formed by the accumulation of alluvial-proluvial deposits in the Quaternary Pleistocene, which is shallow pore water-slightly confined water, with a layer thickness of 10–25 m. The second compression layer comprises Pleistocene alluvial-pluvial layers with a thickness of 15–46 m. The second water-bearing sand layer group is Pleistocene alluvial-proluvial deposits, which constitute deep pore confined water, with a layer thickness of 30–48 m. The semi-cemented layer is formed by accumulating Neogene alluvial-proluvial deposits and flood slope deposits. The part with a burial depth of less than 150 m is water-rich semi-cemented loose sandstone, which can be used as a part of the deep confined aquifer group. Hard clay or clay rock buried below 150 m can be used as the water-repellent floor of the deep pore water confined aquifer group. The bedrock comprises Carboniferous Permian coal-measure strata and Jurassic red sandstone, which are relatively stable rock layers buried under loose layers in this area.

Hydrogeology

Pore water in the study area is mainly affected by atmospheric precipitation infiltration, groundwater exploitation, lateral runoff recharge, and river water seepage. Regional water levels are controlled by seasonal precipitation and groundwater extraction. The primary source of pore water recharge in this area is the infiltration of atmospheric precipitation, followed by lateral runoff, river water seepage, and irrigation back infiltration. The main discharge methods are groundwater extraction, lateral runoff, and evaporation.

The annual water level varies with the amount of precipitation (Fig. 2). Generally, the pore water is mainly excavated and excreted manually from April to June. The water level continues to drop, resulting in a low water level period. From July to November, the infiltration of pore water is dominated by atmospheric precipitation, the water level rises rapidly, and a period of high water level occurs. In areas outside the influence range of the precipitation funnel formed by groundwater extraction, the pore water level basically fluctuates within a specific range for many

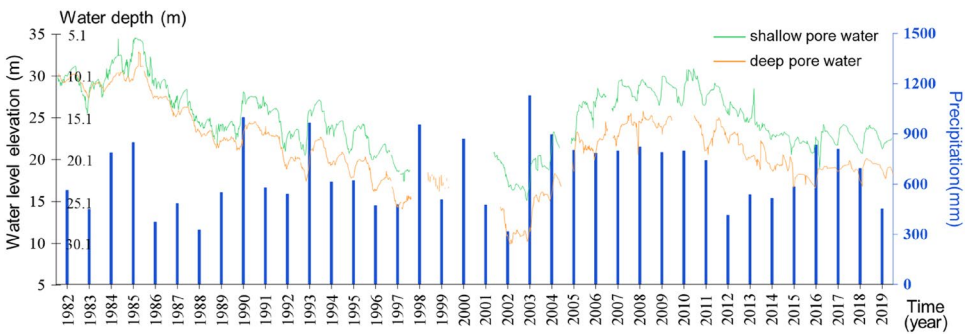

Fig. 2 The relationship between annual water level elevation and precipitation

years. In the study area, the groundwater level generally declined with the massive extraction of groundwater.

Human engineering activities

The second aquifer is the study area's main exploitation layer of groundwater. Mining wells are mainly distributed in Suzhuang water source, Chengbei water source, Fenghuangtai water source, Shaokanghu water source, Chengnan water source, South waterworks, and North waterworks (see Fig. 3 for the location of water sources). It also includes rural water source wells and enterprise-owned wells (the wells here are scattered, so they are not marked in Fig. 3 but can be seen in the numerical simulation model). The coal mines in the study area are mainly the Daizhuang coal mine and some working faces of the Tangkou coal mine. The Daizhuang coal mine is mined at two levels, − 410 m and − 415 m, with a mining thickness of about 3 m. The Tangkou coal mine is excavated at − 750 m, in which the thickness is about 2.1–10.7 m, with an average of 3 m.

By comparing the InSAR data from 2019 to 2020(Fig. 4), there are overlapping groundwater and coal mining areas in the study area. The land subsidence in the Fenghuangtai area is mainly caused by the Tangkou coal mine and the Fenghuangtai water source. Land subsidence in the Shaokanghu area is driven primarily by the Daizhuang coal mine and the water source of Shaokanghu.

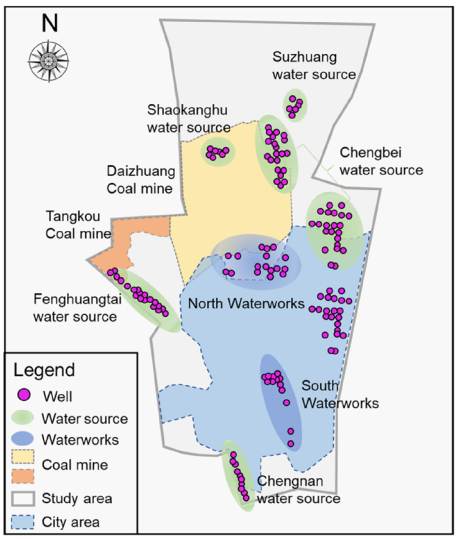

Fig. 3 Location of water sources and mining areas in the study area

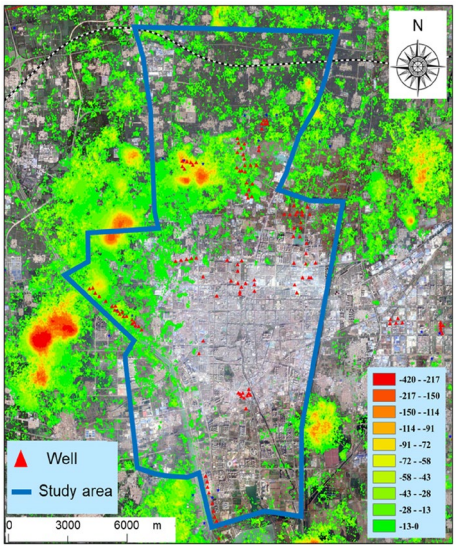

Fig. 4 InSAR data from 2019 to 2020 in the study area

Material and methods

Numerical mode

Due to the irregular shape of the study area, the model of the study area is expanded outward into a rectangular area to prevent problems in the meshing of the model and avoid the influence of irregular boundaries on the calculation results. Here, the size of the expanded rectangular area is about 465 km^2. According to the lithology of the stratum, the stratum was generalized into 15 layers in the vertical direction. The Quaternary loose layer has a depth of − 200 m and is generalized into seven layers. The bedrock and coal seam range is from − 200 to − 800 m, generalized to 8 layers. The physical and mechanical parameters of the rock and soil mass are shown in Table 1.

The primary groundwater extraction layer in the study area is the second aquifer. The mining wells, including rural water source wells and enterprise-owned wells, are mainly distributed in the Suzhuang water source, the Chengbei water source, the Fenghuangtai water source, the Shaokanghu water source, and the Chengnan water source (Fig. 3). Here, the location distribution of mining wells is shown in Fig. 5b. The operating time of mining wells is considered in the simulation.

The coal mines in the study area are mainly the Daizhuang coal mine and parts of the Tangkou coal mine (Fig. 5a). The Daizhuang coal mine is primarily mined at − 410 m and − 415 m, with an average thickness of 3 m. At the same time, the Tangkou coal mine is mainly mined at − 750 m. with an average thickness of 3 m. The working faces of all mining areas in the study area are generalized, the roadways in the mining area are ignored, and the

Table 1 Physical and mechanical parameters of various stratum

Stratum	Thickness (m)	Young's modulus (MPa)	Poisson's ratio	Density (kg/m^3)	Porosity	Permeability coefficient (m/s)
Topsoil	5	120	0.3	1950	0.47	$3e^{-6}$
First compression layer	13	60	0.3	2000	0.42	$4e^{-7}$
First water-bearing sand group	32	150	0.35	2100	0.35	$1e^{-5}$
Second compression layer	25	65	0.3	2030	0.40	$4e^{-10}$
Second water-bearing sand group	35	180	0.35	2150	0.37	$2e^{-5}$
Semi-cemented aquifer	40	200	0.35	2150	0.40	$1e^{-5}$
Semi-cemented clay layer	50	60	0.2	2100	0.42	$1e^{-10}$
Sandstone 1	90	$3.2e^3$	0.19	2550	–	–
Mudstone 2	10	$1.3e^3$	0.22	2560	–	–
Sandstone 3	110	$3.0e^3$	0.2	2180	–	–
Mudstone 4 (including coal seam)	40	$1.6e^3$	0.23	2500	–	–
Coal seam	4	$0.48e^3$	0.25	1400	–	–
Sandstone 5	50	$2.5e^3$	0.2	2300	–	–
Mudstone 6	65	$1.5e^3$	0.24	2590	–	–
Sandstone 7 (including coal seam)	235	$2.3e^3$	0.2	2320	–	–

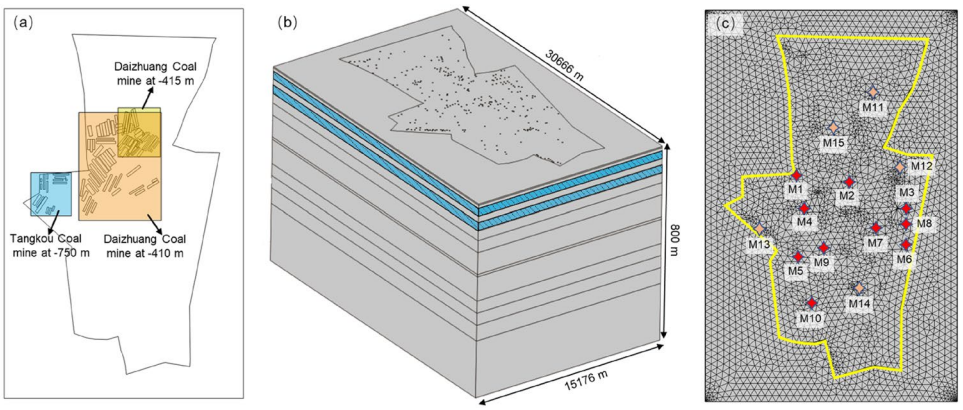

Fig. 5 3D numerical model, **a** layout of the coal mining area, **b** layout of the mining wells, **c** location of the fifteen monitoring points

excavation time of each working face is not considered when modeling.

The diameter of the production well is negligible compared with the model area, so the line element is used to simulate the production wells. The whole model consists of 202,093 mesh elements, 73,074 boundary elements, and 10,884 edge elements. The three-dimensional numerical model and meshing of the tenfold magnification of the thickness are shown in Fig. 5b and Fig. 5c. To verify the accuracy of the model and then investigate the evolution processes, features, and control of land subsidence, 15 monitoring points are set up on the surface of the study area. Among them, the M1–M10 measuring points are consistent with the actual field land subsidence monitoring points. The M11–M15 measurement points are located within the water sources. M11 point is located in the Suzhuang water source, M12 point is situated in the Chengbei water source, M13 point is located in the Fenghuangtai water source, M14 point is situated in the Chengnan water source, and the M15 point is located in the Shaokanghu area. The location of each monitoring point is shown in Fig. 5c.

Numerical model boundary conditions

(1) Initial settlement conditions: take 2000 as the initial settlement time, and assume that the vertical displacement at any point is zero.
(2) Displacement boundary condition: the upper surface is set as a free boundary. The model is surrounded by roller supports to limit the horizontal displacement. The bottom surface is a fixed boundary, limiting the horizontal and vertical displacement.
(3) Water head and flow boundary conditions: Due to the lack of boundary water head monitoring data, the water

head boundary condition of the aquifer is artificially set as the water level buried depth. The rest of the boundaries are set as no-flow boundaries. The mining wells are all flow boundaries, which convert the production volume into linear mass source application.

Numerical model accuracy verification

The study area's ten monitoring points (M1–M10) are used to verify the model's accuracy. Due to the lack of continuous field monitoring data, only the measured settlements in 2016–2017 and 2017–2020 are extracted from the limited data. Compared with the measured data and the simulated results, the simulated values of settlements are in good agreement with the measured values (Fig. 6). In addition, the simulation result from 2019 to 2020 is also compared with the InSAR monitoring data. The results show that the subsidence range is also in good agreement (Fig. 7). Therefore, the above numerical model is valid and can be used for further analysis.

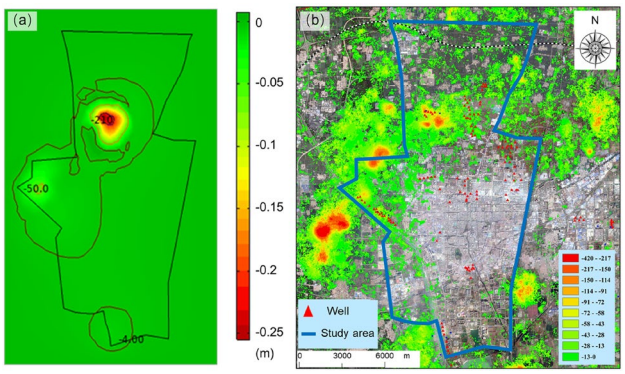

Fig. 7 Comparison between numerical simulation result and InSAR data in 2019–2020

Land subsidence control scheme

To effectively control land subsidence, three groundwater extraction schemes are proposed. The advantages and disadvantages of each scheme are evaluated by comparing and analyzing the impact of different groundwater

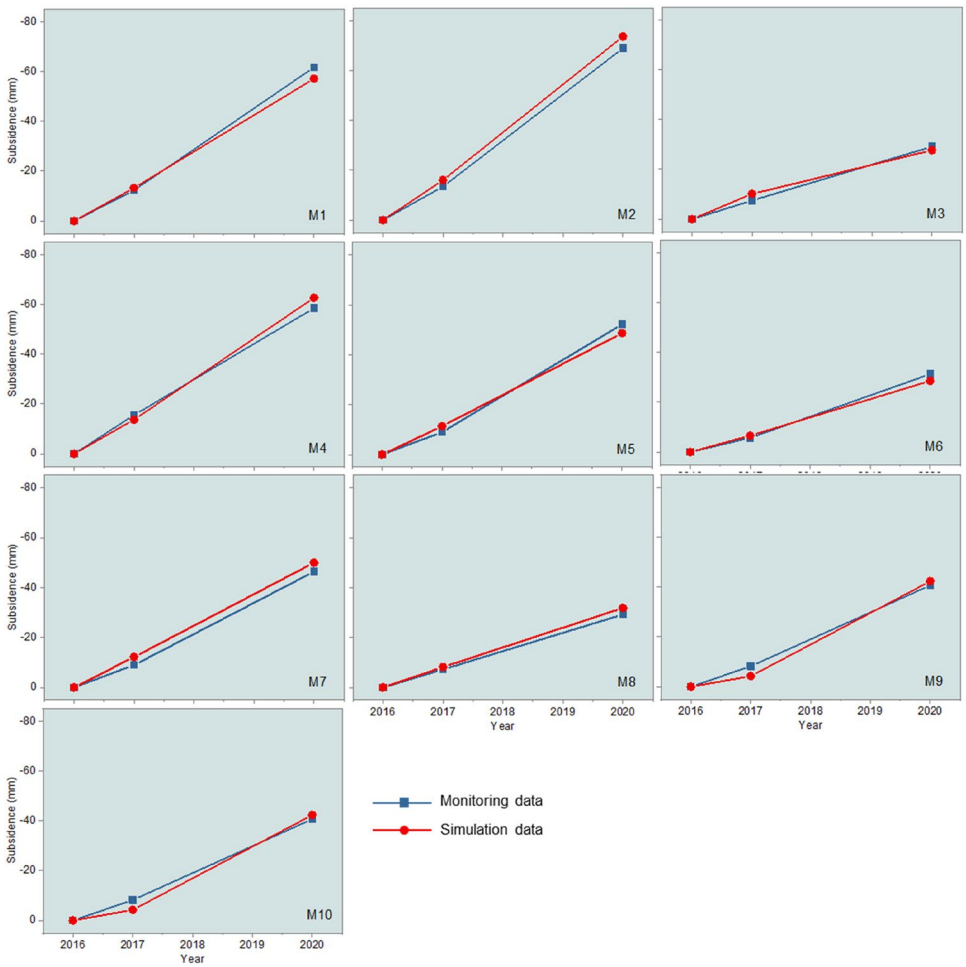

Fig. 6 Comparison between measured data and simulated data of 10 monitoring points

extraction schemes on land subsidence. Here, coal mining is stopped after 2020. Only groundwater extraction is carried out in three extraction schemes. Scheme 1 will keep the original mining wells unchanged from 2021, and schemes 2 and 3 will change the number of extraction wells from 2021(Table 2). In scheme 2, the amount of groundwater discharged of the 52 closed wells is 1500 m^3/d, and that of the remaining ten closed wells is 2400 m^3/d. In scheme 3, the amount of groundwater discharged of the 16 closed wells is 2400 m^3/d. In particular, each extraction scheme is based on the previous scheme and then shuts down more mining wells additionally.

Land subsidence processes and features from 2000 to 2020

Based on the established three-dimensional numerical model, the evolution process of land subsidence in the study area from 2000 to 2020 was simulated. Combined with the mining sequence of wells in water sources such as Suzhuang water source, Chengbei water source, Fenghuangtai water source, Shaokanghu water source, Chengnan water source, South Waterworks, and Beishuiworks, as well as the mining conditions of Daizhuang coal mine and Tangkou coal mine, the land subsidence processes and characteristics of the study area in the past 20 years were analyzed. Figure 8 shows the overall land subsidence of the study area, in which Figs. 8a ~ 8f are the cumulative settlement values and Fig. 8h–m are the cumulative settlement values within a certain period.

Overall, during the past 20 years, the range of land subsidence was concentrated in the location of water sources and coal mining areas, especially in the overlapping regions. The amount of land subsidence and the range of subsidence both showed an increasing trend. In addition, the overlapping regions were the concentrated area of land subsidence, with the most severe land subsidence (Fig. 8). It can be seen from Fig. 8a and h that the land subsidence from 2000 to 2002 was mainly concentrated in the northern part of the city, because the water source wells in the study area gradually shifted to the north and northeast of the urban area. Figures 8b and j show that from 2000 to 2004, the northern part of the city was still the concentrated settlement area. Since the Daizhuang coal mine has mined a new coal face since 2002, the most significant cumulative land subsidence was focused on the Daizhuang coal mine area. Compared with the land subsidence caused by groundwater mining, the land subsidence induced by coal mining accounted for the central part of the land subsidence during this period (Fig. 8i).

Figures 8c and d show that from 2004 to 2012, due to the newly opened mining wells in the north and south of the

Table 2 Groundwater exploitation schemes

Scheme[a]	Urban water source wells	Rural water source wells	Enterprise-owned wells
1	All 124 wells are mined	All wells are mined	All wells are mined
2	Close 62 wells (located in North waterworks, South waterworks, and Chengbei water source)	All wells are mined	All wells are mined
3	Close 16 of the remaining 62 wells (located in Chengbei water source)	All wells are mined	All wells are mined

[a]Each extraction scheme is based on the previous scheme and then shuts down more mining wells additionally

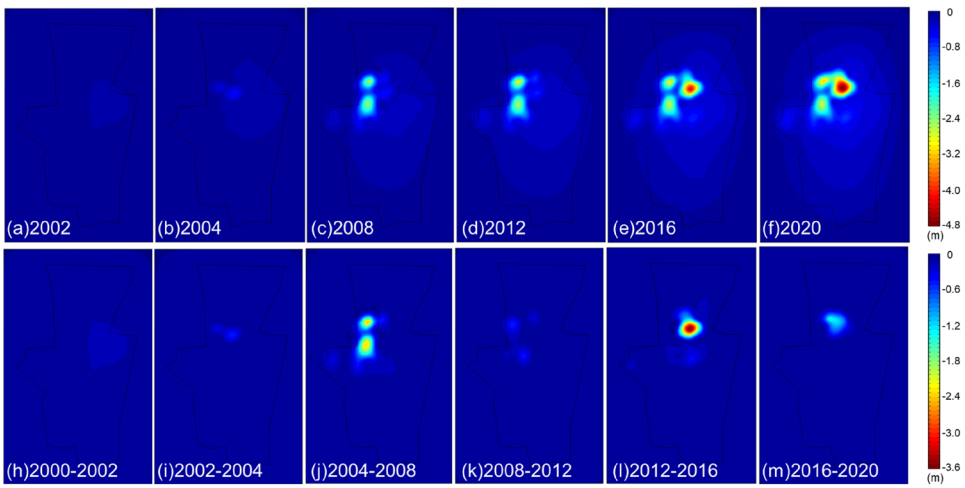

Fig. 8 Land subsidence evolution from 2000 to 2020, **a–f** are the cumulative settlement values, and **h–m** are the cumulative settlement values within a certain period

city, the land subsidence range in the study area increased and showed a trend of gradually decreasing from north to south. The largest cumulative subsidence area was still concentrated in the Daizhuang coal mine area, which was obviously caused by the combination of coal mining and groundwater mining. Compared to 2004, the land subsidence maximum point in 2012 shifted caused by the newly mined working face of the Daizhuang coal mine and Tangkou coal mine (Fig. 8j and k). From 2012 to 2016, new mining wells were opened in the Suzhuang water source, Chengbei water source, and Chengnan water source, which led to the continuous increase of land subsidence in the study area. But the increasing rate gradually decreased from north to south (Fig. 8e). Compared to 2012, the new working face mined in Daizhuang coal mine from 2012 to 2016 resulted in the shift of the maximum subsidence point in 2016. However, the maximum cumulative land subsidence was still concentrated in the Dai Zhuang coal mine area (Fig. 8i).

Since both Daizhuang coal mine and Tangkou coal mine had new mining working faces from 2016 to 2020, the scope of land subsidence upon the goaf continued to expand. The subsidence caused by the gob in Daizhuang coal mine showed a trend of connectivity (Fig. 8f). However, during 2016–2020, the coal mine did not have a large area of new working face, so the increasing rate of land subsidence in 2016–2020 was lower than that in 2012–2016 (Fig. 8m).

In general, the land subsidence showed a trend of high in the north and low in the south during 2000–2020. The evolution process of land subsidence in 20 years was closely related to groundwater and coal mining planning. The numerical simulation results show that, in a short period, the impact of coal mining on land subsidence is more significant than that of groundwater mining. However, with the passage of the coal face, the land subsidence in the mining area has been completed and gradually controlled by groundwater mining.

Analysis of land subsidence control

Land subsidence has a significant impact on human activities. For coal mining, new energy can be used to replace coal resources to meet the city's energy needs at this stage. However, the life of residents and the city's development are inseparable from groundwater. How to reasonably balance the relationship between groundwater exploitation and land subsidence has an essential impact on the economic development of the study area. Therefore, this section analyzes and evaluates the groundwater exploitation scheme under the groundwater exploitation scheme proposed in "Land subsidence control scheme", with land subsidence as the evaluation index.

Analysis of land subsidence under scheme 1

Based on the existing groundwater exploitation conditions before 2020, new mining wells were opened in the Shaokanghu water source in 2020. Based on the numerical model established in "Material and methods", the land subsidence of the study area from 2021 to 2030 was analyzed. Figures 9a–d show the study area's cumulative land subsidence

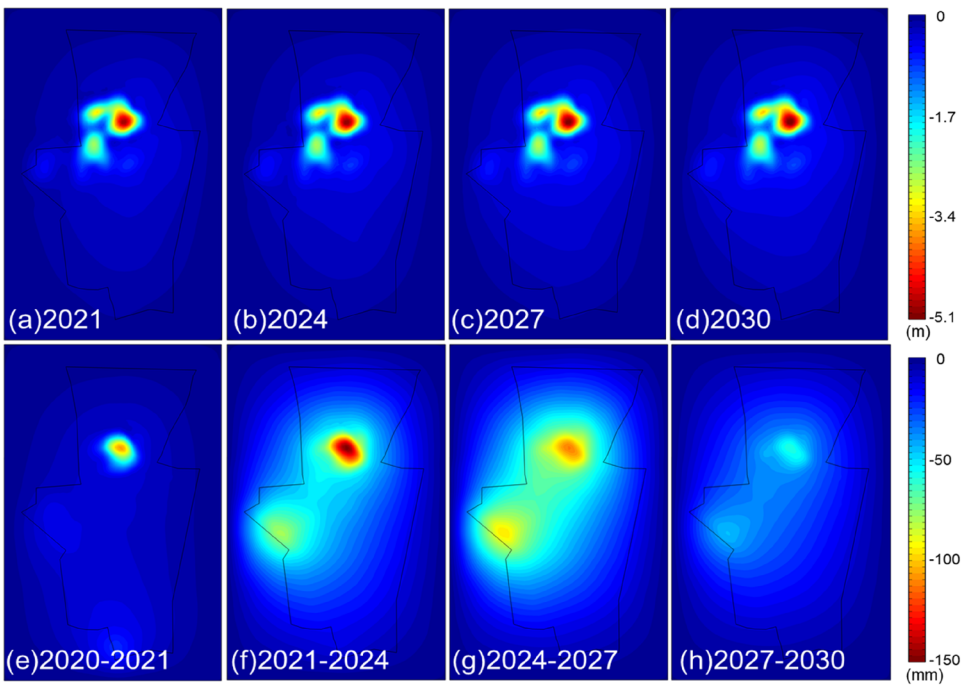

Fig. 9 Land subsidence evolution under scheme one from 2021 to 2030, **a–d** are the cumulative settlement values, and **e–h** are the cumulative settlement values within a certain period

in 2021, 2024, 2027, and 2030, respectively. Figures 9e–h are the cumulative subsidence within a certain period.

Figure 9 shows that if the current mining status were maintained, the cumulative amount of land subsidence and the range of land subsidence in the study area would continue to increase in the next ten years, which significantly impact urban development. Since Daizhuang coal mine did not added new mining faces after 2021, the maximum position of total land subsidence did not change. Suppose no measures were taken to control land subsidence, the maximum cumulative land subsidence reached 5.10 m, located at the overlap of the − 410 m and − 415 m coal mining in the Daizhuang coal mine. From 2021 to 2024, the 3 year cumulative subsidence at the maximum subsidence point was 104.63 mm, and the annual average subsidence rate was 34.88 mm/a. Significant land subsidence occurred in the Shaokanghu water source, which tended to be connected with the subsidence area of the Daizhuang coal mine (Fig. 9f). Figure 9g shows that in 2024–2027, the accumulated subsidence at the maximum subsidence point was 94.24 mm. The land subsidence had slowed in the past three years, and the annual average subsidence rate was 31.41 mm/a. This area was basically connected with the land subsidence area of Shaokanghu. The three-year cumulative subsidence at the maximum subsidence point from 2027 to 2030 was 50.80 mm, the cumulative subsidence continued to decrease, and the annual average subsidence rate was 16.93 mm/a (Fig. 9h).

Table 3 shows the settlement of monitoring points M1–M10 during 2021–2030. Land subsidence will continue to occur at each monitoring point from 2021 to 2030. Over time, the subsidence rate of each monitoring point slowed down in the three years from 2027 to 2030. From 2021 to 2030, although Daizhuang Coal Mine and Tangkou Coal Mine had stopped mining, they still impacted the land subsidence, but the subsidence rate continued to decrease with time. In 2020, new mining wells were opened in the water source of Shaokanghu. The land subsidence rate in the Shaokanghu area was relatively large initially and reached its peak in 2027. However, with the passage of time, the consolidation degree of the aquifer layer increased, and the land subsidence rate slowed down.

Table 3 Land subsidence under scheme 1 in the study area from 2021 to 2030

Monitoring point	Cumulative settlement (mm)			
	2021	2024	2027	2030
M1	− 1405.42	− 1455.60	− 1519.81	− 1555.32
M2	− 588.77	− 634.68	− 693.83	− 727.20
M3	− 285.65	− 305.57	− 331.38	− 346.96
M4	− 523.21	− 578.12	− 647.26	− 684.63
M5	− 245.45	− 295.28	− 356.39	− 388.71
M6	− 214.74	− 231.73	− 252.99	− 266.21
M7	− 329.60	− 357.36	− 392.92	− 414.40
M8	− 253.47	− 272.27	− 296.38	− 311.16
M9	− 294.11	− 336.38	− 388.95	− 418.29
M10	− 205.75	− -232.94	− 263.85	− 281.78

Analysis of land subsidence under scheme 2

In scheme 2, 62 production wells in the south waterworks, the north waterworks and Chengbei water source were designed to close in 2021, and the land subsidence from 2021 to 2030 was predicted based on the numerical model. Figures 10a–d show the cumulative land subsidence of the study area in 2021, 2024, 2027, and 2030 under scheme 2, respectively. Figures 10e–h are the cumulative subsidence within a certain period.

Figure 10 shows that shutting down the wells had a good control effect on land subsidence. In the beginning, the ground started to rebound. After the seepage field affected by groundwater exploitation was dynamically balanced, the land subsidence continued to occur slowly. In the 10 year forecast period, the land subsidence in the study area can be divided into two stages. One is the ground rebound stage that occurs on the ground in some areas of the mining wells, and the second stage is that the land subsidence continues to occur after the rebound stage slowly.

After directly shutting down 62 wells, Fig. 10b and f show that the region where the mining wells were closed experienced a significant rebound between 2021 and 2024. The maximum land subsidence point located in Daizhuang coal mine was affected by the closed wells in the city's northern area. The three-year cumulative ground rebound amount reached 30.54 mm, and the annual average rebound rate reached 10.18 mm/a. After 2024, the ground rebound effect began to diminish. The land subsidence in the Daizhuang coal mine and Shaokanghu water source (water mining began in 2021) continued to develop, and there was a trend of connectivity (Fig. 10c and g). Subsidence continued to occur at the maximum land subsidence area, with a cumulative subsidence of 80.57 mm from 2024 to 2027 and an annual average subsidence rate of 26.86 mm/a. Figure 10d and h show that after 2027, the land subsidence in the Shaokanghu water source and the Daizhuang coal mine, which was the core area, began to slow down, but the accumulated subsidence continued to increase. By 2030, the maximum total subsidence in the study area reached 4.98 m, which was still located at the overlap of the − 410 m and − 415 m coal mining in the Daizhuang coal mine. From 2027 to 2030, at the maximum subsidence point, the three-year cumulative subsidence amount was 51.77 mm, and the annual average subsidence rate was 17.26 mm/a.

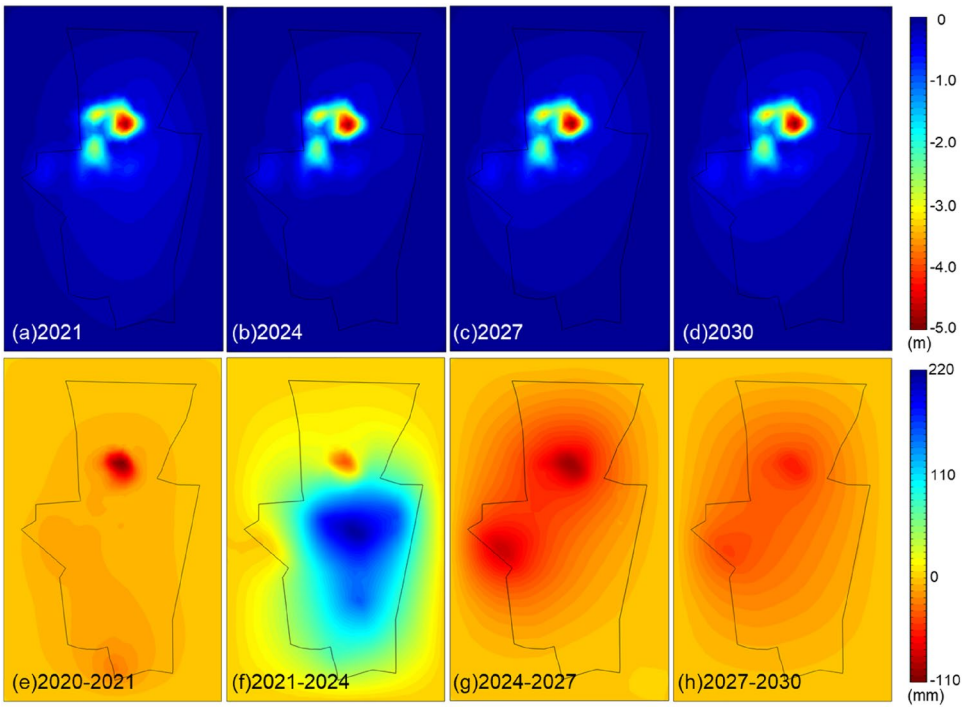

Fig. 10 Land subsidence evolution under scheme 2 from 2021 to 2030, **a**–**d** are the cumulative settlement values, and **e**–**h** are the cumulative settlement values within a certain period

Table 4 Land subsidence under scheme 2 in the study area from 2021 to 2030

Monitoring point	Cumulative settlement (mm)			
	2021	2024	2027	2030
M1	− 1404.85	− 1309.43	− 1358.98	− 1395.57
M2	− 588.25	− 420.78	− 462.93	− 497.06
M3	− 285.47	− 142.21	− 156.92	− 172.69
M4	− 522.64	− 392.32	− 445.20	− 483.56
M5	− 245.19	− 166.69	− 212.95	− 246.02
M6	− 214.76	− 105.02	− 115.28	− 128.51
M7	− 329.45	− 159.18	− 179.02	− 200.71
M8	− 253.36	− 124.77	− 137.54	− 152.42
M9	− 293.91	− 169.05	− 204.92	− 234.82
M10	− 206.44	− 122.61	− 140.90	− 159.02

Table 4 shows the settlement of monitoring points M1–M10 in 2021–2030 under scheme 2. For the closure of 62 production wells in 2021, the ground rebound occurred at all monitoring points from 2021 to 2024. The ground rebound rate and amount are more significant at the monitoring points close to the closed wells, whereas the ground rebound rate and ground rebound amount are smaller. After 2024, land subsidence continued at each monitoring point, but the subsidence rate slowed down.

Analysis of land subsidence under scheme 3

Scheme 3 is to close further 16 mining wells in the Chengbei water source based on scheme 2. The land subsidence from 2021 to 2030 was predicted based on the numerical model. Figures 11a–d show the cumulative land subsidence of the study area in 2021, 2024, 2027, and 2030 under Scheme 3, respectively. Figures 11 are the cumulative subsidence within a certain period.

It can be seen from Fig. 11 that the land subsidence trend of scheme 3 was basically the same as scheme 2 in general. That is, in the next ten years, the ground rebound occurred first in the study area, and then the land subsidence continued. Compared with scheme 2, since 16 more water source wells were shut down in scheme 3, the rebound rate and total rebound of the ground in the early stage of ground rebound increased to a certain extent (Table 5). By 2030, the cumulative maximum total subsidence in the study area reached 4.87 m, with a decrease of 110 mm compared with scheme 2. It was still located at the overlap of the − 410 m and − 415 m coal mining in the Daizhuang coal mine (Fig. 11d). From 2021 to 2024, the three-year cumulative rebound at the maximum cumulative settlement point increased significantly, reaching 128.86 mm. The annual average springback rate reached 42.95 mm/a (Fig. 11b and Fig. 11f). Compared with scheme 2, and there was a significant increase. From 2024 to 2027, subsidence continued to occur at the point of maximum cumulative subsidence, with a cumulative land subsidence of 76.34 mm and an annual average subsidence rate of 25.45 mm/a during the three

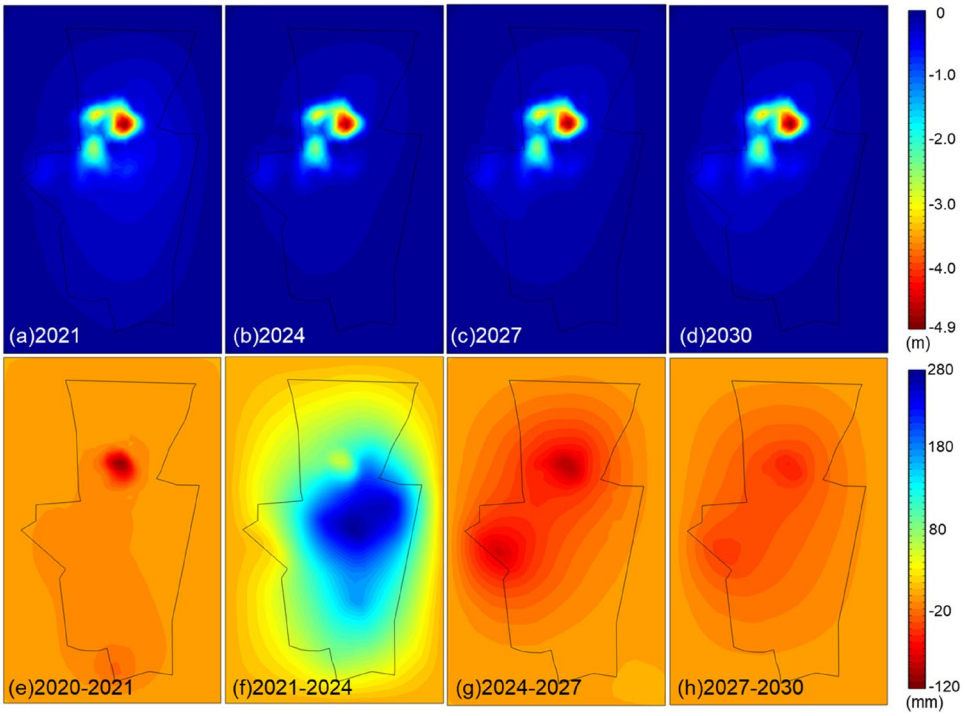

Fig. 11 Land subsidence evolution under scheme 3 from 2021 to 2030, **a**–**d** are the cumulative settlement values, and **e**–**h** are the cumulative settlement values within a certain period

Table 5 Land subsidence under scheme 3 in the study area from 2021 to 2030

Monitoring point	Cumulative settlement (mm)			
	2021	2024	2027	2030
M1	− 1404.46	− 1263.78	− 1310.36	− 1344.91
M2	− 587.37	− 338.08	− 377.28	− 409.28
M3	− 284.61	− 85.70	− 99.08	− 113.69
M4	− 522.16	− 351.41	− 401.43	− 437.71
M5	− 245.03	− 142.72	− 186.78	− 218.16
M6	− 214.43	− 73.21	− 82.38	− 94.59
M7	− 328.87	− 111.07	− 129.07	− 149.18
M8	− 252.79	− 80.52	− 92.03	− 105.79
M9	− 293.64	− 137.64	− 171.30	− 199.43
M10	− 206.48	− 108.12	− 124.99	− 141.94

Table 6 Land subsidence under different mining schemes to 2030

Monitoring point	Cumulative settlement in 2030 (mm)		
	Scheme 1	Scheme 2	Scheme 3
M1	− 1555.32	− 1395.57	− 1344.91
M2	− 727.20	− 497.06	− 409.28
M3	− 346.96	− 172.69	− 113.69
M4	− 684.63	− 483.56	− 437.71
M5	− 388.71	− 246.02	− 218.16
M6	− 266.21	− 128.51	− 94.59
M7	− 414.40	− 200.71	− 149.18
M8	− 311.16	− 152.42	− 105.79
M9	− 418.29	− 234.82	− 199.43
M10	− 281.78	− 159.02	− 141.94

years (Fig. 11c and g). The subsidence area of Daizhuang coal mine and Shaokanghu water source had a noticeable connection trend. From 2027 to 2030, the three-year cumulative subsidence at the maximum cumulative subsidence point was 49.10 mm, and the annual average subsidence rate was 16.37 mm/a. Compared with scheme 2, the accumulated settlement was slightly lower.

Table 5 shows the settlement of M1–M10 monitoring points in 2021–2030 under scheme 3. Due to the closure of 78 mining wells in the north and south of the city in 2021, the ground rebound occurred at each monitoring point in the study area from 2021 to 2024, and the amount of rebound was more significant than scheme 2. Similarly, the ground rebound rate and ground rebound amount were more prominent at the monitoring point close to the closed well. In contrast, the ground rebound rate and ground rebound amount were lower. After 2024, land subsidence continued to occur at each monitoring point, and the final total subsidence was less than scheme 2.

Comparative analysis of control schemes

Table 6 shows the cumulative subsidence of M1–M10 monitoring points during 2000–2030 under different mining schemes. When 62 production wells were closed in 2021, the total amount of groundwater discharged was 102,000 m^3/d. Compared with scheme 1, the final cumulative settlement

values of measuring points M1–M10 decreased by 10.27, 31.65, 50.23, 29.37, 36.71, 51.73, 51.57, 51.02, 43.86, and 43.57%. When 78 production wells were shut down in 2021, the total amount of groundwater discharged was 140,400 m^3/d. Compared with scheme 1, the final cumulative settlement values of measuring points M1–M10 decreased by 13.53, 43.72, 67.23, 36.07, 43.88, 64.47, 64.00, 66.00, 52.32 and 49.63%. In general, stopping groundwater extraction can effectively control land subsidence. Comparing scheme 2 and scheme 3, it is found that the more shut-down wells (i.e., the more groundwater discharge), the better the control effect of land subsidence, the more significant the reduction of land subsidence, and the smaller the accumulated final total subsidence.

Figure 12 shows the subsidence curve of each water source measuring point (M11–M15) from 2021 to 2030. In scheme 1, the land subsidence rate of each water source was the largest, and the measurement point with the most significant subsidence from 2021 to 2030 was located in the Shaokanghu area, with a settlement of 295.57 mm. In scheme 2, the ground rebound phenomenon occurred at all the five measuring points in the first few years. Still, the rebound rate and amount decreased over time, and then the land subsidence continued. Judging from the cumulative subsidence, the monitoring points of Suzhuang(M11), Fenghuangtai(M13), and Shaokanghu(M15) in 2030 had a certain amount of land subsidence compared with 2021. In 2030, the monitoring points in the Chennan(M12) and Chenbei(M14) had rebounded compared with 2021. This is because the monitoring points in Suzhuang, Fenghuangtai, and Shaokanghu are far away from the closed wells. The monitoring points in Chennan and Chenbei are closer to the closed wells, which is impacted by shutting down wells more significantly.

Under scheme 3, the ground rebound phenomenon occurred in all five measuring points in the first few years. But over time, the rate of rebound and the amount of rebound decreased, and then land subsidence continued. Compared with scheme 2, scheme 3 closed 16 more mining wells in the Chengbei water source and the net increase of the total amount of groundwater discharged was 38,400 m^3/d. The rebound amount of each water source measurement point increased in the first few years, but the following subsequent settlement decreased. In addition, the change in land subsidence was more significant near the closed wells than far from the closed wells. In terms of cumulative subsidence, the Fenghuangtai and Shaokanghu monitoring points in 2030 had experienced a certain amount of land subsidence compared with 2021, while the Suzhuang, Chengbei, and Chengnan monitoring points in 2030 had rebounded compared with 2021.

From the above analysis, it can be seen that under the condition of full well production in scheme 1, the amount of land subsidence continued to increase, and the rate of land subsidence slowed down over time. In general, stopping groundwater extraction can effectively control land subsidence. After comparing the schemes, it is found that the land subsidence is basically stable when the amount of groundwater exploitation wells is closed by 50%, which is a more reasonable and practical exploitation scheme.

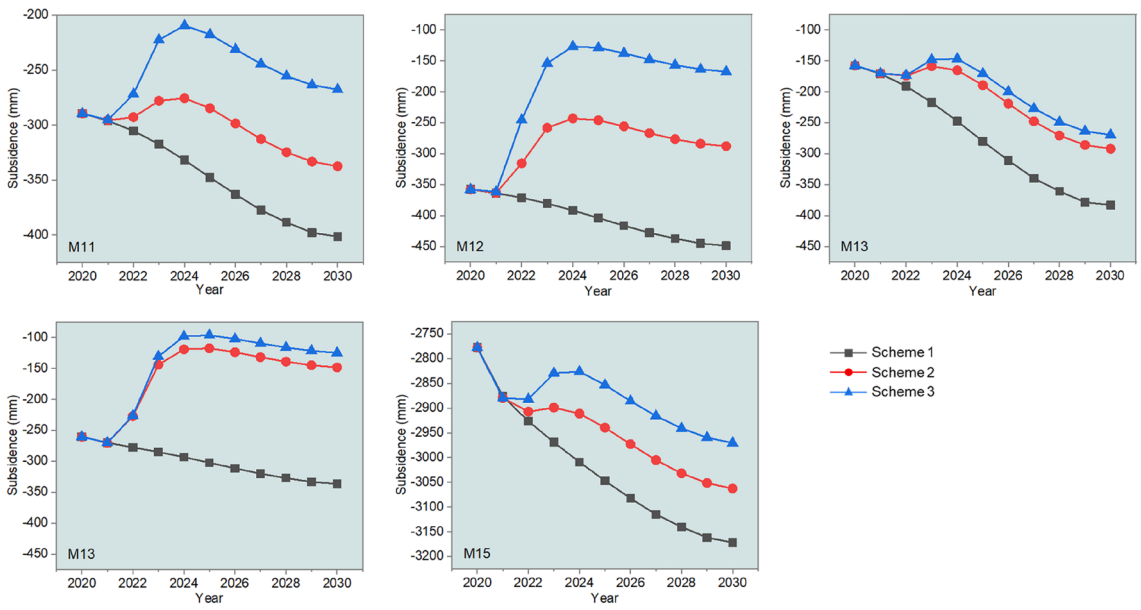

Fig. 12 Comparison of cumulative settlement of each measuring point under different schemes

Limitations and prospects

(1) As an effective method to study land subsidence, numerical simulation can better simulate the characteristics of land subsidence in the study area. However, it is undeniably different from the actual situation. Natural factors such as measurement errors, rainfall, and river recharge can all affect the simulation results. In addition, due to the large number of working faces in the coal mine and the cluttered actual mining time, the established model can only reasonably generalize the number of working faces and the exact mining time. On the other hand, due to a large number of mining wells in the study area and the unclear operation time of some mining wells, the model cannot accurately consider the opening month of the mining wells and can only reasonably generalize the operating years of the mining wells and their mining volumes. In general, by comparing the numerical simulation data of land subsidence with the measured data and InSAR monitoring data in this study, the established three-dimensional numerical model of land subsidence in the study area can better simulate the problems of land subsidence caused by groundwater and coal mining.

(2) Groundwater extraction and coal mining are the leading causes of land subsidence. At present, much research has been carried out on the mechanism of land subsidence under the action of a single factor, and many instructive research results have been obtained. However, like the study area of this paper, land subsidence is obviously affected by the coupling of groundwater extraction and coal mining(Guzy and Witkowski 2021). Currently, the mechanism of land subsidence under the coupling action is still unclear, and it is a direction that needs further research.

(3) How to accurately predict land subsidence is also a hot research topic. Land subsidence data can be obtained using ground monitoring, InSAR, and other technical means(Diao et al. 2018, 2016). Numerical simulation can also be used to acquire land subsidence data for a certain period in the future(Edalat et al. 2020). It is believed that with the development of artificial intelligence, the prediction of land subsidence under the coupling action of groundwater mining and coal mining based on artificial intelligence is also worth studying.

(4) Additionally, as mentioned above, groundwater exploitation and land subsidence are contradictory topics. A crucial and meaningful subject is how to effectively control land subsidence and meet the demand for water resources in the study area. At this stage, there is a real need to study the dynamic regulation mechanism of groundwater exploitation through numerical simulation. At the same time, when large-scale public and transportation facilities need to be built in the subsidence area, it is also necessary to carry out targeted research(Ding et al. 2020; Jia et al. 2021).

Conclusions

Aiming at the problem of land subsidence features and subsidence control under the combined action of groundwater and coal mining, the main groundwater mining area in Jining city was taken as a case study. A three-dimensional numerical model was established to analyze the evolution process of land subsidence caused by groundwater and coal mining in the study area from 2000 to 2020. Based on the control principle of land subsidence in the study area from 2021 to 2030, different schemes for controlling subsidence in the study area were analyzed. The main conclusions are as follows:

(1) A three-dimensional numerical model of groundwater and coal mining land subsidence in the study area was established according to the survey report data, geotechnical test data, water mining, coal mine data, etc. The model's accuracy was verified using InSAR data and field-measured data. The established three-dimensional numerical land subsidence model can reasonably simulate the land subsidence caused by groundwater extraction and coal mining.

(2) Based on the established numerical model, the evolution process of land subsidence in the study area from 2000 to 2020 was simulated. The land subsidence from 2020 to 2030 was also predicted under different schemes. In the past 30 years, the study area's land subsidence showed a trend of high in the north and low in the south. At the same time, the changing trend of land subsidence in the past 30 years was closely related to groundwater extraction and coal mining planning. The maximum cumulative subsidence was located in the overlapping area of − 410 m and − 415 m coal mining in the Daizhuang coal mine. In a short period, the impact of coal mining on land subsidence is significantly more significant than groundwater mining. With the passage of the coal mining surface, the land subsidence in the mining area has been gradually controlled by groundwater mining.

(3) The evolution features of land subsidence under different groundwater exploitation schemes are analyzed and predicted. Reducing the amount of groundwater exploitation can significantly slow down the development rate of land subsidence. Different groundwater exploitation schemes have different effects on land subsidence. According to the current situation of ground-

water exploitation in the study area, the land subsidence is basically stable when the amount of groundwater exploitation wells is closed by 50%, which is a more reasonable and practical exploitation scheme.

(4) Based on this research, it is believed that further research should be carried out on the land subsidence mechanism under the coupling action of groundwater mining and coal mining, the artificial intelligence-based land subsidence prediction method, and the dynamic regulation mechanism of groundwater.

Acknowledgements We have received research support from Shandong provincial Lunan geology and exploration institute for providing geological data and comments on our manuscript. This work was supported by the Foundation of Shandong Provincial Lunan Geology and Exploration Institute (LNYQ202101), the National Natural Science Foundation of China (41877239), and the Natural Science Foundation of Shandong Province (ZR2022QD014 and ZR2019QEE025).

Author contributions Zhiqiang Li and Qiqi Chen wrote the main manuscript text. Yiguo Xue and Daohong Qiu advised the manuscript. Hong Chen, Qiushi Liu, and Fanmeng Kong prepared all the figures. All authors reviewed the manuscript.

Funding Foundation of Shandong Provincial Lunan Geology and Exploration Institute, LNYQ202101, Natural Science Foundation of Shandong Province, ZR2022QD014, National Natural Science Foundation of China, 41877239

Data availability The datasets generated during and/or analyzed during the current study are available from the corresponding author on reasonable request.

Declarations

Conflict of interest The authors have no relevant financial or non-financial interests to disclose.

References

Chen B, Gong H, Li X, Lei K, Zhu L, Gao M, Zhou C (2017) Characterization and causes of land subsidence in Beijing, China. Int J Remote Sens 38:808–826. https://doi.org/10.1080/01431161.2016.1259674

Chen BB, Gong HL, Lei KC, Li JW, Zhou CF, Gao ML, Guan HL, Lv W (2019) Land subsidence lagging quantification in the main exploration aquifer layers in Beijing plain, China. Int J Appl Earth Obs Geoinf 75:54–67. https://doi.org/10.1016/j.jag.2018.09.003

Dehghani M, Zoej MV, Bolourchi M, Shemshaki A, Saatchi S (2008) Monitoring of Hashtgerd land subsidence induced by overexploitation of groundwater using SAR interferometry. Geosciences 17:50–55

Di ST, Jia C, Zhang SP, Ding PP, Shao M, Zhang YW (2020) Regional characteristics and evolutionary trend prediction of land subsidence caused by groundwater over exploitation in North Shandong of the North China Plain. Acta Geol Sin 94:1638–1654

Diao X, Wu K, Hu D, Li L, Zhou D (2016) Combining differential SAR interferometry and the probability integral method for three-dimensional deformation monitoring of mining areas. Int J Remote Sens 37:5196–5212

Diao X, Bai Z, Wu K, Zhou D, Li Z (2018) Assessment of mining-induced damage to structures using InSAR time series analysis: a case study of Jiulong Mine, China. Environ Earth Sci 77:1–14

Ding PP, Jia C, Di ST, Wang LL, Bian C, Yang X (2020) Analysis and prediction of land subsidence along significant linear engineering. Bull Eng Geol Env 79:5125–5139. https://doi.org/10.1007/s10064-020-01872-1

Ebrahimy H, Feizizadeh B, Salmani S, Azadi H (2020) A comparative study of land subsidence susceptibility mapping of Tasuj plane, Iran, using boosted regression tree, random forest and classification and regression tree methods. Environ Earth Sci 79:1–12. https://doi.org/10.1007/s12665-020-08953-0

Edalat A, Khodaparast M, Rajabi AM (2020) Scenarios to control land subsidence using numerical modeling of groundwater exploitation: Aliabad plain (in Iran) as a case study. Environ Earth Sci 79:1–12. https://doi.org/10.1007/s12665-020-09246-2

Gerardo HG, Pablo E, Roberto T, Marta BP, Juan LV, Mauro R, Rosa MM, Dora CF, John L, Pietro T (2021) Mapping the global threat of land subsidence. Science 371:34–36. https://doi.org/10.1126/science.abb854

Guzy A, Malinowska AA (2020a) Assessment of the impact of the spatial extent of land subsidence and aquifer system drainage induced by underground mining. Sustainability 12:7871

Guzy A, Malinowska AA (2020b) State of the art and recent advancements in the modelling of land subsidence induced by groundwater withdrawal. Water 12:2051. https://doi.org/10.3390/w12072051

Guzy A, Witkowski WT (2021) Land subsidence estimation for aquifer drainage induced by underground mining. Energies 14:4658. https://doi.org/10.3390/en14154658

Holzer TL, Galloway DL (2005) Impacts of land subsidence caused by withdrawal of underground fluids in the United States. Hum Geol Agent. https://doi.org/10.1130/2005.4016(08)

Hu R, Yue Z, Wang L, Wang S (2004) Review on current status and challenging issues of land subsidence in China. Eng Geol 76:65–77. https://doi.org/10.1016/j.enggeo.2004.06.006

Jia C, Yang X, Wu J, Ding PP, Bian C (2021) Monitoring analysis and numerical simulation of the land subsidence in linear engineering areas. KSCE J Civ Eng 25:2674–2689. https://doi.org/10.1007/s12205-021-1823-x

Liu BC, Yang JS, Zhang JS (1999) Surface subsidence and deformation caused by open pit mining and dewatering. J China Coal Soc 24:41–44

Mehdi BG, Seiyed Mossa H, Behzad AA, Yasamin S, Homa E, Faezeh M, Shervin A (2021) Land subsidence: a global challenge. Sci Total Environ 778:146193. https://doi.org/10.1016/j.scitotenv.2021.146193

Peng J, Sun X, Wang W, Sun G (2016) Characteristics of land subsidence, earth fissures and related disaster chain effects with respect to urban hazards in Xi'an, China. Environ Earth Sci 75:1–15. https://doi.org/10.1007/s12665-016-5928-3

Phien-wej N, Giao PH, Nutalaya P (2006) Land subsidence in bangkok, Thailand. Eng Geol 82:187–201. https://doi.org/10.1016/j.enggeo.2005.10.004

Shen SL, Xu YS (2011) Numerical evaluation of land subsidence induced by groundwater pumping in Shanghai. Can Geotech J 48:1378–1392. https://doi.org/10.1139/t11-049

Xue YQ, Zhang Y, Ye SJ, Wu JC, Li QF (2005) Land subsidence in China. Environ Geol 48:713–720. https://doi.org/10.1007/s00254-005-0010-6

Yang Y, Song XF, Zheng FD, Liu LC, Qiao XJ (2015) Simulation of fully coupled finite element analysis of nonlinear hydraulic properties in land subsidence due to groundwater pumping.

Environ Earth Sci 73:4191–4199. https://doi.org/10.1007/s12665-014-3705-8

Zhang Y, Liu YL, Jin MQ, Jing Y, Liu Y, Liu YF, Sun W, Wei JQ, Chen YY (2019) Monitoring land subsidence in Wuhan city (China) using the SBAS-InSAR method with radarsat-2 imagery data. Sensors 19:743. https://doi.org/10.3390/s19030743